Vibration suppression of a flywheel system using a novel nonlinear vibration absorber with an Euler buckled beam

Liu Haiping, Shi Wenhua

Beijing Institute of Spacecraft System Engineering, Beijing, China

E-mail: lhpvibration@163.com

Abstract. The micro-vibration from flywheel system, as one of the main disturbances, has restricted the effective use of high sensitive payloads in satellites. In order to suppress the low-frequency line spectrum from the flywheel, a novel nonlinear vibration absorber (NVA) using Euler buckled beam is developed. The proposed NVA is attached on the supporting structure of the flywheel assembly, aiming to attenuate the line spectrum introduced by the flywheel in operation. A discrete multi-degree-of-freedom dynamic model, which includes the NVA, the flywheel and the supporting structure by taking into account of the gyroscopic effect of the flywheel, is built. The NVA is represented by a linear positive stiffness spring and parallel Euler buckled beams. The systematic dynamic equations with and without the NVA under the micro-vibration from the flywheel, respectively, are solved by using fourth-order Runge-Kutta method in time-domain. In addition, the effects of initial imperfection, oblique angle and damping coefficient of the Euler buckled beam on the vibration suppression performance are studied. The calculating results reveal that a typical nonlinear dynamic absorber for controlling the micro-vibration from the flywheel is constructed successfully based on the provided designing parameters of the Euler buckled beam. Compared with the vibration responses of the combined system with and without the NVA, it can be concluded that the NVA has better attenuation performance. The initial imperfection and damping coefficient of the Euler buckled beam exist optimum values, and with the increase of the oblique angle, the vibration controlling characteristics of the NVA have been improved.

1. Introduction

The micro-vibration from flywheel, as one of the main disturbances, has severe influence on the characteristics of high sensitive payloads in satellites. A large number of studies have investigated the producing mechanisms of the micro-vibration from the flywheel. The researchers have conducted substantial studies on the flywheel in the field of empirical and analytical disturbance models in [1-5], and have presented a method to measure disturbing force and momentum by using a Kistler platform. According to the research on the producing mechanisms in [6, 7], interactions between the same two types of the flywheels [8] and the flywheel-supporting structure [9], the dynamic characteristics and the coupling mechanisms of the micro-vibration have been proposed.

At present, some isolating devices, which have been used in micro-vibration suppression in satellites, exhibit limited effects on micro-vibration control due to the low frequency disturbances located in the vicinity of the turning frequency of the isolating system [10]. These low frequency disturbances are mainly originated from coupling resonances when the rotary speed of the flywheel equals to the natural frequency of spinning rotor considering the gyroscopic effects.

Comparing with the linear vibration absorber, the NVA exhibits some merits, such as absorbing vibrations over a broadband, high efficiency in vibration control, relatively small mass, and without the need for additional energy in [11, 12]. The designing frequency of vibration control devices in spacecraft need relatively broad spectrum due to strict restriction in the field of payloads' weight, energy consumption, and complicated cases in the phases of launching and working in the orbit.

In an author's published paper [13], some comparison for the vibration controlling characteristics have been made between the NVA and an optimum linear vibration absorber under multi-frequency excitation, the performance of the former on broad frequency band is more excellent.

To begin with, the models of a single flywheel and the flywheel-supporting structure coupling system are provided by considering the gyroscopic effect in this paper, respectively. And then a novel NVA is built by using the Euler buckled beam, and a discrete multi-degree-freedom dynamic model, which represents the flywheel-NVA-supporting structure system, is constructed. Thirdly, the non-linear dynamic equations are solved by using fourth-order Runge-Kutta method under the excitation from the flywheel in time-domain. Finally, the effects of initial imperfection, oblique angle and damping coefficient of the Euler buckled beam on the vibration suppression performance are studied.

2. Dynamic modelling

2.1. The model of the flywheel

Flywheel mainly includes three types of vibrational modes, that is, translation in axial direction, translation in two radial directions and rocking along radial direction. Due to the manufacturing error, flywheel exists imbalance during the operating process. Flywheel imbalance is generally the largest disturbance source and causes a disturbance force and torque when the wheel in operation. There are two kinds of flywheel imbalances, static and dynamic. Static imbalance results from the offset of the centre of mass of the wheel from its spin axis, and dynamic imbalance is caused by the misalignment of the wheel's principle axis and the rotation axis.

The simple analytical model of the flywheel is exhibited, as shown in Figure 1. The spring element $k_r/2$ represents the supporting stiffness of the flywheel structure. The damping element $c_r/2$ represents the equivalent damping coefficient for the shaft and bearings. The parameter d represents the distance from the centre of the wheel for the stiffness and damping elements. The elements M and R represent the flywheel mass and radius, respectively. In addition, the symbols θ and ϕ represent the rotating angles along radial direction, respectively. And the coordinates x and y are the radial translation, respectively.

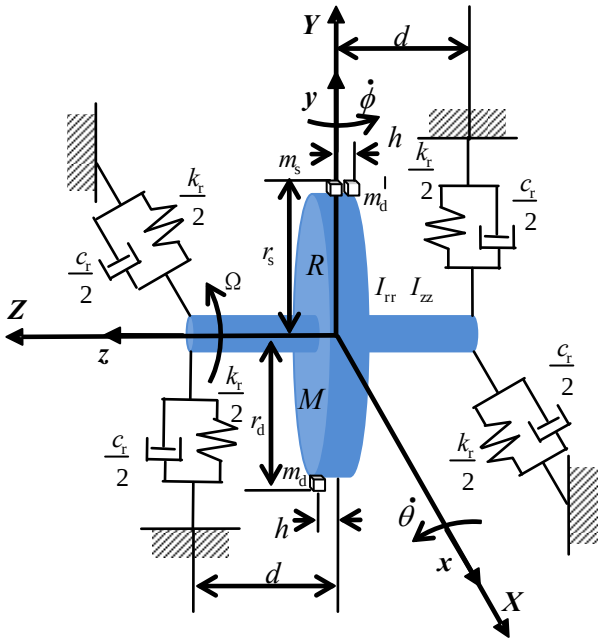

Figure 1. Schematic of the flywheel model ([2, 5])

For simplicity, it is assumed that θ, ϕ, x, y are all small values. Using the assumption of symmetry in the model, the dynamic equations of the flywheel can be expressed as follows:

$$\begin{bmatrix} M & 0 \\ 0 & M \end{bmatrix}\begin{Bmatrix} \ddot{x} \\ \ddot{y} \end{Bmatrix}+\begin{bmatrix} c_r & 0 \\ 0 & c_r \end{bmatrix}\begin{Bmatrix} \dot{x} \\ \dot{y} \end{Bmatrix}+\begin{bmatrix} k_r & 0 \\ 0 & k_r \end{bmatrix}\begin{Bmatrix} x \\ y \end{Bmatrix}=\begin{Bmatrix} 0 \\ 0 \end{Bmatrix} \tag{1-a}$$

$$\begin{bmatrix} I_{rr} & 0 \\ 0 & I_{rr} \end{bmatrix}\begin{Bmatrix} \ddot{\theta} \\ \ddot{\phi} \end{Bmatrix}+\begin{bmatrix} c_\theta & \Omega I_{zz} \\ -\Omega I_{zz} & c_\theta \end{bmatrix}\begin{Bmatrix} \dot{\theta} \\ \dot{\phi} \end{Bmatrix}+\begin{bmatrix} k_\theta & 0 \\ 0 & k_\theta \end{bmatrix}\begin{Bmatrix} \theta \\ \phi \end{Bmatrix}=\begin{Bmatrix} 0 \\ 0 \end{Bmatrix} \tag{1-b}$$

where the torsional stiffness $k_\theta=k_r d^2$, the torsional damping $c_\theta=c_r d^2$, the radial moment of inertia $I_{rr}=MR^2/2$, the polar moment of inertia $I_{zz}=MR^2/4$.

Static imbalance is caused by the offset of the centre of mass of the flywheel from the axis of rotation. It can be modelled by using a small mass, m_s, placed at a radius, r_s, as shown in [5]. The static imbalance is defined as $U_s=m_s r_s$.

Dynamic imbalance is caused by angular misalignment of the principle axis of the wheel and the spin axis. It can be modelled by using two equal masses, m_d, placed 180^0 apart at a radial distance, r_d, and a distance h from the centre of the flywheel. The dynamic imbalance is defined as $U_d=2m_d r_d$.

The systematic equations of motion which include the static and dynamic imbalance and the higher harmonics are governed by:

$$\begin{bmatrix} M_t & 0 \\ 0 & M_t \end{bmatrix}\begin{Bmatrix} \ddot{x} \\ \ddot{y} \end{Bmatrix}+\begin{bmatrix} c_r & 0 \\ 0 & c_r \end{bmatrix}\begin{Bmatrix} \dot{x} \\ \dot{y} \end{Bmatrix}+\begin{bmatrix} k_r & 0 \\ 0 & k_r \end{bmatrix}\begin{Bmatrix} x \\ y \end{Bmatrix}=\begin{Bmatrix} -U_s\Omega^2\sin(\Omega t)-\sum_{i=2}^{n} C_i\Omega^2\sin(h_i\Omega t) \\ U_s\Omega^2\cos(\Omega t)+\sum_{i=2}^{n} C_i\Omega^2\cos(h_i\Omega t) \end{Bmatrix} \tag{2}$$

$$\begin{bmatrix} I_{rr} & \alpha \\ \alpha & I_{rr} \end{bmatrix}\begin{Bmatrix} \ddot{\theta} \\ \ddot{\phi} \end{Bmatrix}+\begin{bmatrix} c_\theta & \Omega I_{zz} \\ -\Omega I_{zz} & c_\theta \end{bmatrix}\begin{Bmatrix} \dot{\theta} \\ \dot{\phi} \end{Bmatrix}+\begin{bmatrix} k_\theta & 0 \\ 0 & k_\theta \end{bmatrix}\begin{Bmatrix} \theta \\ \phi \end{Bmatrix}=\begin{Bmatrix} U_d\Omega^2\cos(\Omega t)+\sum_{i=2}^{n}C_i\Omega^2\cos(h_i\Omega t) \\ U_d\Omega^2\sin(\Omega t)+\sum_{i=2}^{n}C_i\Omega^2\sin(h_i\Omega t) \end{Bmatrix} \tag{3}$$

where the total mass of the flywheel $M_t = M + m_s + 2m_d$, $\alpha = \left(2m_d r_d^2 + m_s r_s^2\right)\sin(2\Omega t)/2$.

2.2. The coupling model of the flywheel-supporting structure

In practice, the flywheel is usually fixed on the aluminum honeycomb sandwich plate, as shown in Figure 2. The coupling model of the flywheel-supporting structure is also presented in Figure 2. The linear springs and the lumped masses are employed to express the dynamic characteristics of the supporting structure and the flywheel, respectively.

The coupling dynamic equations of the flywheel-supporting structure are:

$$\begin{bmatrix} M_t & 0 \\ 0 & M_m \end{bmatrix}\begin{Bmatrix} \ddot{y}_t \\ \ddot{y}_m \end{Bmatrix}+\begin{bmatrix} c_r & -c_r \\ -c_r & c_m \end{bmatrix}\begin{Bmatrix} \dot{y}_t \\ \dot{y}_m \end{Bmatrix}+\begin{bmatrix} k_r & -k_r \\ -k_r & k_m \end{bmatrix}\begin{Bmatrix} y_t \\ y_m \end{Bmatrix}=\begin{Bmatrix} 0 \\ f_t \end{Bmatrix} \tag{4}$$

where M_t and M_m represent the mass of the flywheel system and the aluminum honeycomb sandwich plate, respectively. y_t and y_m represent the displacement of the supporting structure and the flywheel, respectively. k_r represents the supporting stiffness of the flywheel structure and c_r represents the equivalent damping coefficient for the shaft and bearings. k_m and c_m represent the modal stiffness and structural damping coefficient for the fixed-fixed aluminum honeycomb sandwich plate, respectively. f_t represents the external excitation.

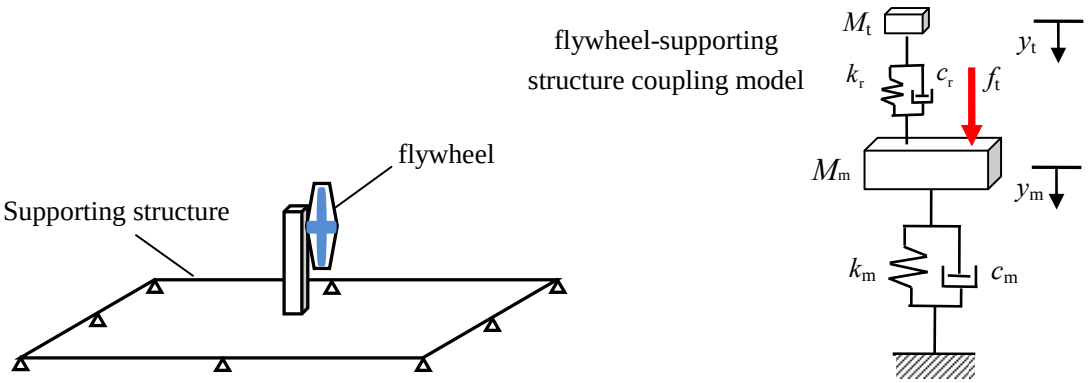

Figure 2. Schematic of the flywheel-supporting structure coupling model

2.3. The model of the NVA

The studied NVA is constructed by the negative stiffness beam structure, the linear spring and the lumped mass, which is shown in Figure 3. Four Euler buckled beams are used as a negative corrector. Meanwhile, a linear spring is fixed under the lumped mass which provides a relatively small stiffness to cancel the effect from the weight of the lumped mass.

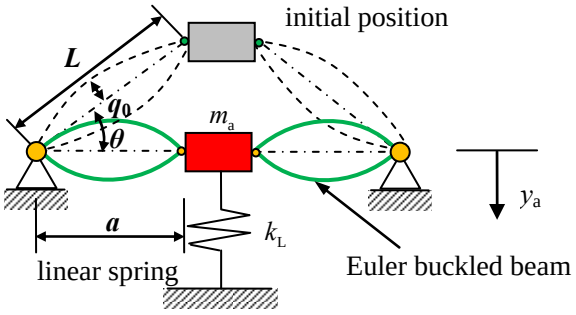

Figure 3. Schematic of the NVA

The horizontal position of the lumped mass is assumed to be the equilibrium state. The relationship between force and displacement of the NVA can be derived:

$$F = k_L L\left[k_1'\frac{y_a}{L} + k_3'\left(\frac{y_a}{L}\right)^3 + \sqrt{1-\gamma^2}\right] - m_a g \tag{5}$$

where F is the restoring force of the absorbing system, k_L is the linear spring stiffness, h_a is the sectional height of the Euler beam, w is the sectional width of the Euler beam, m_a is the mass of the NVA, g is the gravitational acceleration, $P_e=EI(\pi/L)^2$ is the critical buckling load of Euler beam with hinged-hinged boundary, EI is the bending rigidity of the beam, $\gamma=\cos\theta$, $I = wh_a^3/12$. $k_1=[(a-b)/a\gamma](b_2/2-2\gamma+6)$ and $k_3=(a-b)/a\gamma+[(a-b)/2\gamma^3a+b/\gamma^2a^3](b^2/2-2\gamma+6)$, $k_1' = 1-\lambda k_1$ and

$k_3' = \lambda k_3$, $k_L L\sqrt{1-\gamma^2} = m_a g$, $b=\pi q_0/L$ and $\lambda=P_e/k_L L$ are the parameters defined for simplicity.

2.4. The model of the flywheel-NVA-supporting structure

A combined model of the flywheel and the NVA on the supporting structure, as shown in Figure 4, is developed in order to investigate the effects of the NVA on the micro-vibration from the flywheel.

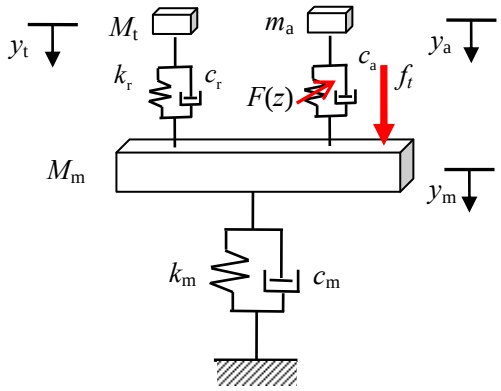

Figure 4. Schematic of the flywheel-NVA-supporting structure model

The combined system equations can be obtained:

$$\begin{cases} M_{\mathrm{m}}\ddot{y}_{\mathrm{m}}+c_{\mathrm{m}}\dot{y}_{\mathrm{m}}+k_{\mathrm{m}}y_{\mathrm{m}}+c_{\mathrm{a}}\left(\dot{y}_{\mathrm{m}}-\dot{y}_{\mathrm{a}}\right)+k_{\mathrm{L}}L\left[k_1'\dfrac{y_{\mathrm{m}}-y_{\mathrm{a}}}{L}+k_3'\left(\dfrac{y_{\mathrm{m}}-y_{\mathrm{a}}}{L}\right)^3+\sqrt{1-\gamma^2}\right] \\ -m_{\mathrm{a}}g+k_{\mathrm{r}}\left(y_{\mathrm{m}}-y_{\mathrm{t}}\right)+c_{\mathrm{r}}\left(\dot{y}_{\mathrm{m}}-\dot{y}_{\mathrm{t}}\right)=f_{\mathrm{t}} \\ m_{\mathrm{a}}\ddot{y}_{\mathrm{a}}+c_{\mathrm{a}}\left(\dot{y}_{\mathrm{a}}-\dot{y}_{\mathrm{m}}\right)+k_{\mathrm{L}}L\left[k_1'\dfrac{y_{\mathrm{a}}-y_{\mathrm{m}}}{L}+k_3'\left(\dfrac{y_{\mathrm{a}}-y_{\mathrm{m}}}{L}\right)^3+\sqrt{1-\gamma^3}\right]-m_{\mathrm{a}}g=0 \\ M_{\mathrm{t}}\ddot{y}_{\mathrm{t}}+k_{\mathrm{r}}\left(y_{\mathrm{t}}-y_{\mathrm{m}}\right)+c_{\mathrm{r}}\left(\dot{y}_{\mathrm{t}}-\dot{y}_{\mathrm{m}}\right)=0 \end{cases} \tag{6}$$

3. Results and Discussion

3.1. Parameters for the calculations

The flywheel parameters used in calculations are listed in Table 1. They are used to represent a typical flywheel, as shown in [4]. The relating initial designing values of the supporting structure and the NVA are listed in Table 2.

Table 1. Parameter values of the flywheel model [4]

Parameters	Values	Units
Flywheel mass, M_{t}	5.9	kg
Polar MOI, I_{zz}	0.075	kg·m^2
Radial MOI, I_{rr}	0.063	kg·m^2
Lateral stiffness, k_{r}	5.24×10^6	N/m
Imbalance radial distance, d	0.16	m
Lateral damping coefficient, c_{r}	0	Ns/m
Static imbalance, U_{s}	0.716	g·cm
Dynamic imbalance, U_{d}	29.54	g·cm^2
Imbalance radial distance, $r_{\mathrm{s}}/r_{\mathrm{d}}$	0.16	m

Table 2. Initial parameter values of the NVA and the supporting structure

Parameters	Values	Units	
Mass, M_{m}	10	kg	Main vibrator (Supporting structure)
Modal stiffness, k_{m}	1.01×10^7	N/m	
Damping coefficient, c_{m}	0	Ns/m	
Mass of the absorber, m_{a}	0.1	kg	Euler buckled beam
Linear stiffness, k_{L}	3×10^2	N/m	
Damping coefficient, c_{a}	10	N·s/m	
Initial length, L	0.02	m	
Initial imperfection, q_0	1×10^{-3}	m	
Young's modulus, E	210	GPa	
Sectional height of the Euler beam, h_{a}	1×10^{-4}	m	
Sectional width of the Euler beam, w	1×10^{-3}	m	
Initial oblique angle, θ	10	°	

3.2. Free oscillations

Assuming that the initial values of the designing variables as follows: $y_{\mathrm{m}}(0)=y_{\mathrm{t}}(0)=y_{\mathrm{a}}(0)=0$, $\dot{y}_{\mathrm{t}}(0)=\dot{y}_{\mathrm{a}}(0)=0$, $\dot{y}_{\mathrm{m}}(0)=3\mathrm{m/s}$.

The free oscillations of the flywheel-NVA-supporting structure system are investigated by using the model in Figure 4. The responses of the flywheel-supporting structure with and without the NVA as shown in Figure 5 where the expressions in equation (6) have been calculated by using the fourth-order Runge-Kutta method. For comparison the effects of the NVA on the dynamic performance of the flywheel-supporting structure system, it is assumed that the parameter c_m equals to 0 Ns/m.

Figure 5 displays the transfer of energy from the flywheel and the supporting structure to the NVA. In the case where the damping c_m is not present and a beating phenomenon appears for the mass of the supporting structure and the flywheel, respectively, as shown in Figure 5(a) and 5(b). It can be found that the non-linear energy pumping occurs in the range of t=0s∼0.5s, as shown in Figure 5(c). The energy pumping phenomenon corresponds to a controlled one-way channelling of the vibrational energy to a passive nonlinear structure where it localized and diminishes in time due to damping dissipation. In addition, the input energy from the main vibrational structure to the NVA should satisfy a specific threshold to excite the energy pumping phenomenon. It can be seen that the energy pumping phenomenon disappeared when the amplitude of the main vibrational structure smaller than a certain value at about t=0.5s, as shown in Figure 5(c).

3.3. Forced oscillations

It can be seen that the disturbing force in radial direction when the flywheel rotates at 6000r/min (RPM) in time domain, as shown in Figure 6(a). And the Power Spectral Density (PSD) from the time-domain flywheel disturbance data is plotted in Figure 6(b).

The disturbance from the flywheel along radial direction as inputting load is exerted on the supporting structure. The calculating results from the components of the flywheel-supporting structure with and without the NVA are exhibited in Figure 7. It is evident that the responses of the supporting structure and the flywheel are suppressed due to using the NVA. However, compared with the results from Figure 6(c) and Figure 7(c), it can be seen obviously that the non-linear energy pumping do not appeared. The primary reason is that the transfer energy from the flywheel disturbance smaller than the previous case, refer to Figure 5.

According to the previous analysing results in [13], the oblique angle, the initial imperfection and the damping coefficient of the Euler buckled beam are the key factors to determine the dynamic performances of the NVA. Thus, the non-linear energy pumping will be excited by changing the values above these three factors when keeping other designing parameters unchanged.

The influences of the damping coefficient (c_m=0Nm/s, 10Nm/s and 500Nm/s) on the dynamic characteristics of the supporting structure are plotted in Figure 8. The PSD of the supporting structure (y_m) decreases with the increase of the damping coefficient above the first resonance frequency at about 16Hz. And when the damping coefficient equals to 500 Nm/s, the PSD exhibits the decreasing trend with the increase of the frequency. Apparently, corresponding to this damping coefficient value, the non-linear energy sink occurs, as indicated by the curves shown in Figure 8.

Figure 9 and Figure 10 show the calculating results for different values of the oblique angle and the initial imperfection. Figure 9 reveals the PSD of the supporting structure for different oblique angle of the Euler buckled beam. Apparently, a smaller or a larger value (θ=5° or θ=15°) of the oblique angle leads to increase of the PSD. It can be concluded that the oblique angle exists the optimum value in the field of vibration control. And the suppression effect of the NVA gets better with the increase of the initial imperfection, as shown in Figure 10.

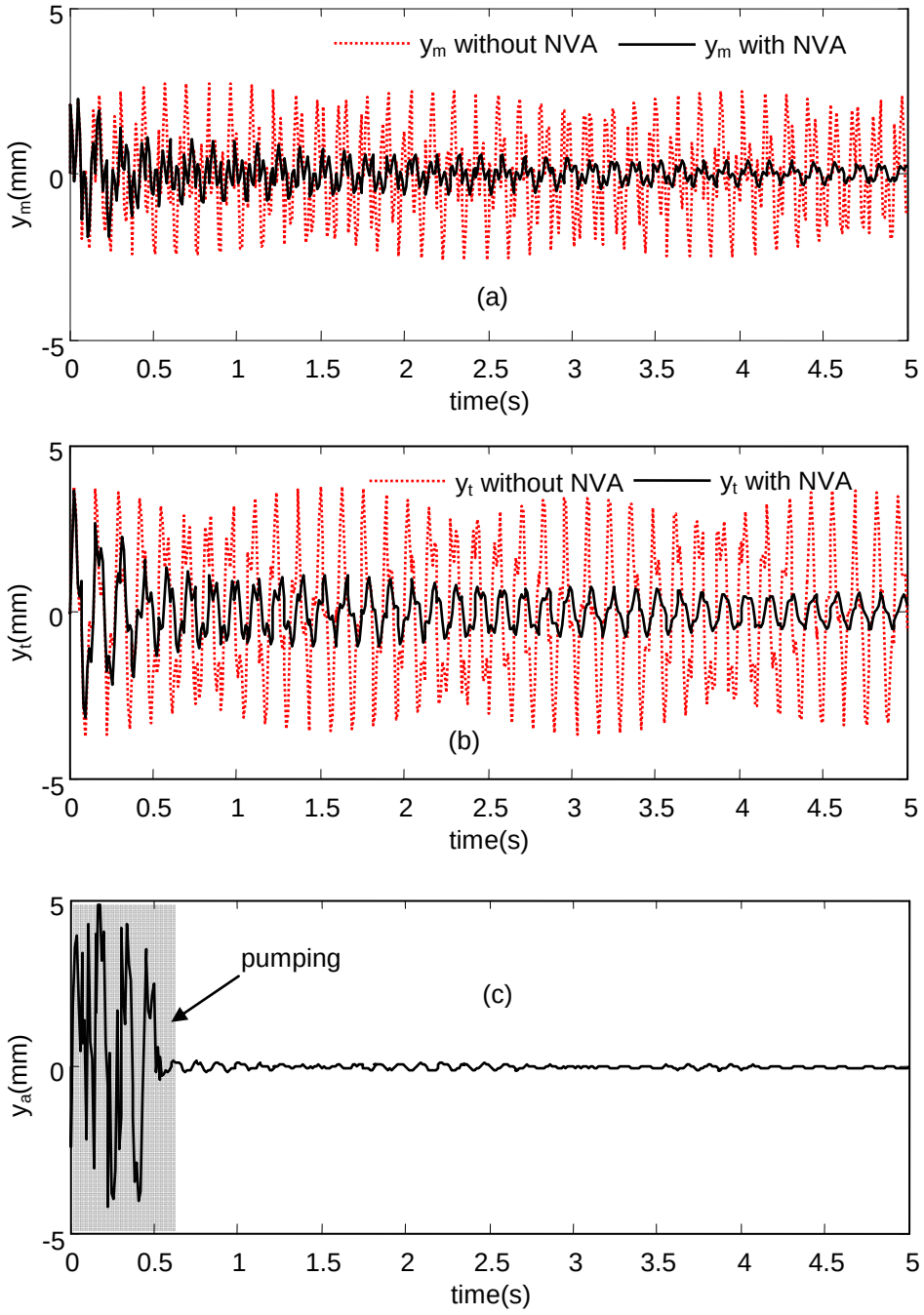

Figure 5. Free oscillations with a non-null initial velocity of the primary structure, (a) y_m with and without the NVA; (b) y_t with and without the NVA; (c) y_a.

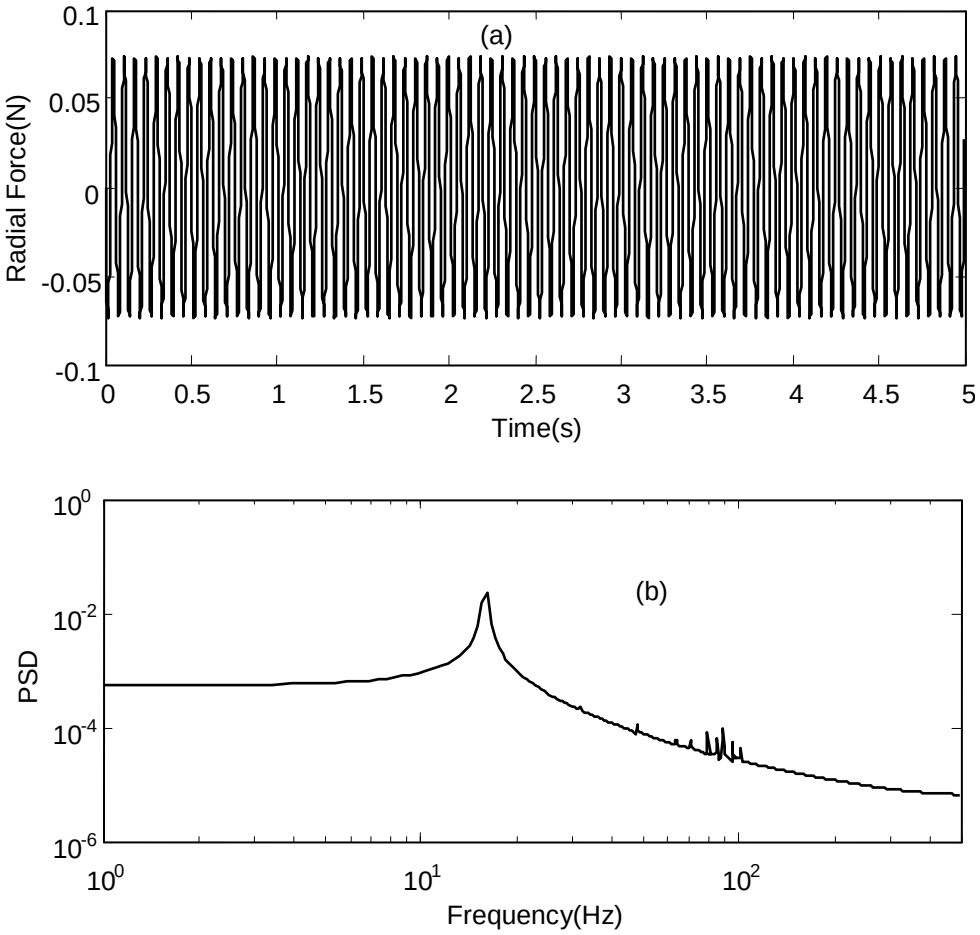

Figure 6. Radial disturbance of the flywheel: (a) time histories; (b) PSD.

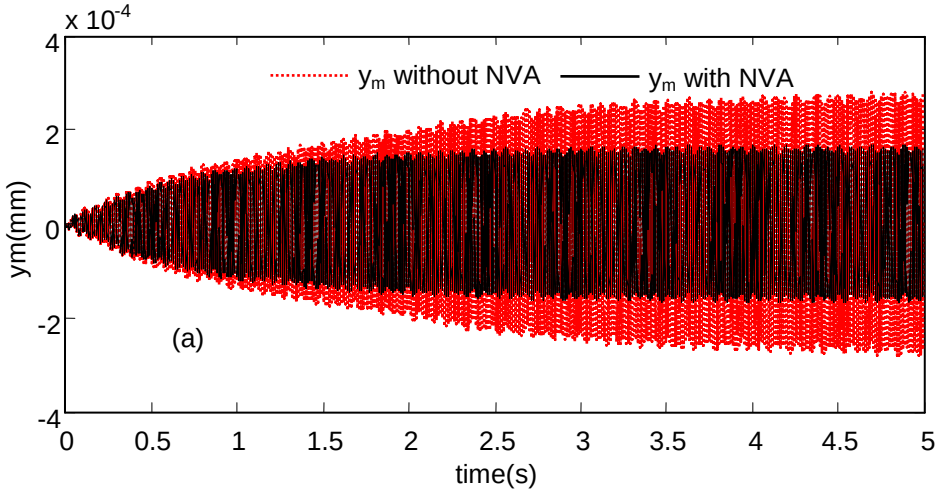

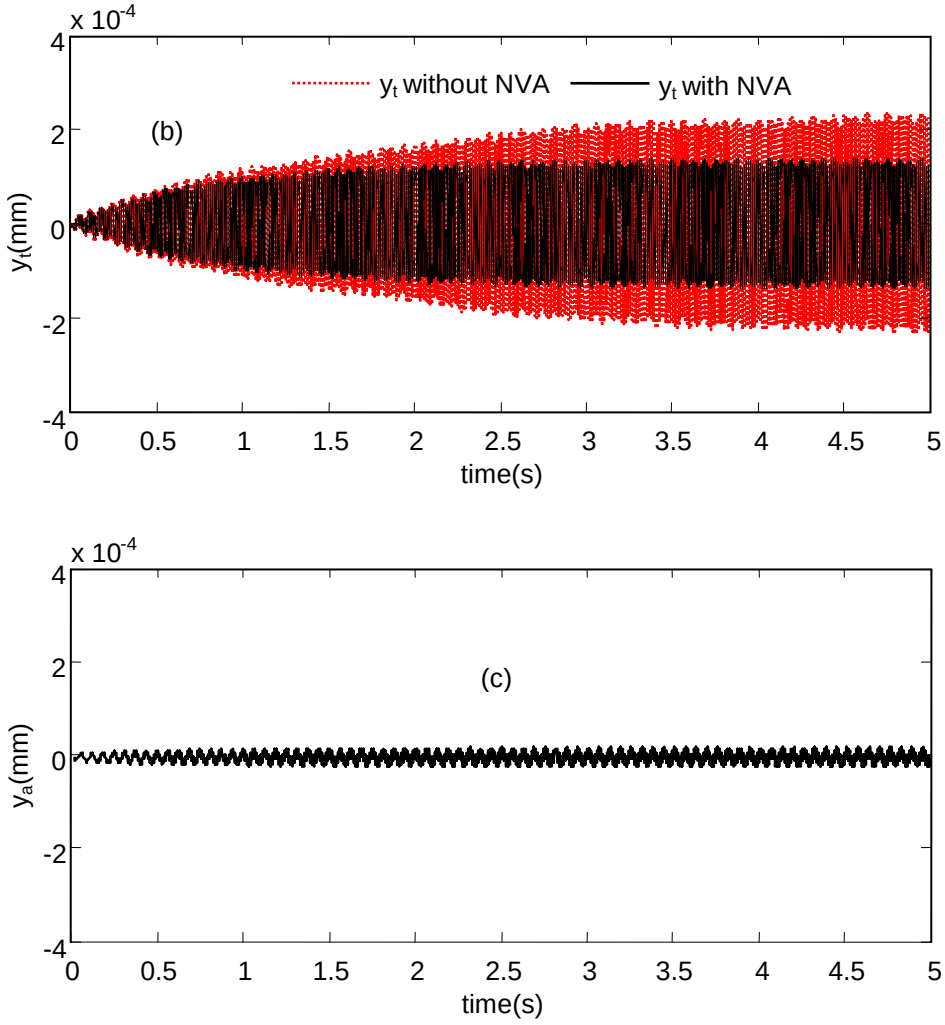

Figure 7. Responses of the coupling system under forced oscillations, (a) y_m with and without the NVA; (b) y_t with and without the NVA; (c) y_a.

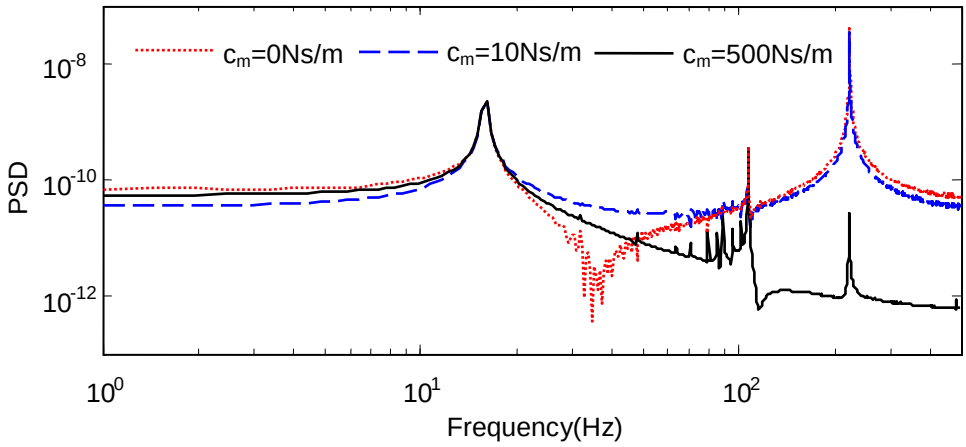

Figure 8. The effects on PSD of the primary structure for different values of c_m.

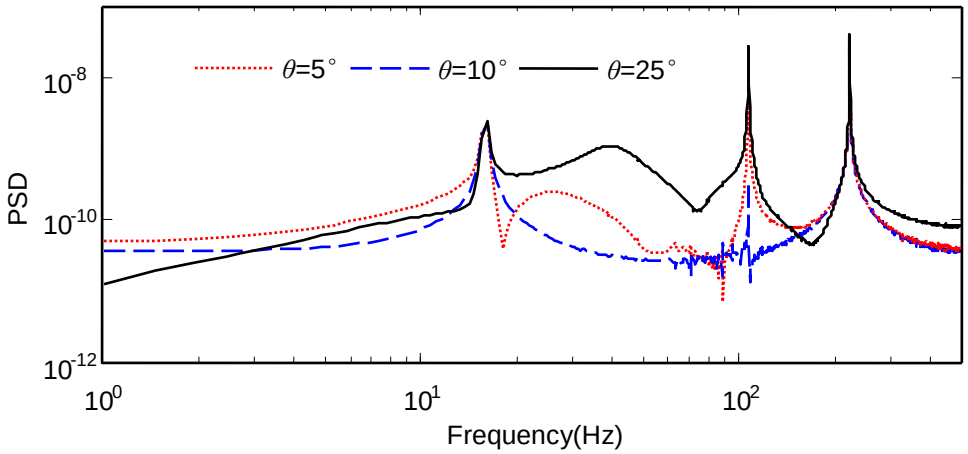

Figure 9. The effects on PSD of the primary structure for different values of θ.

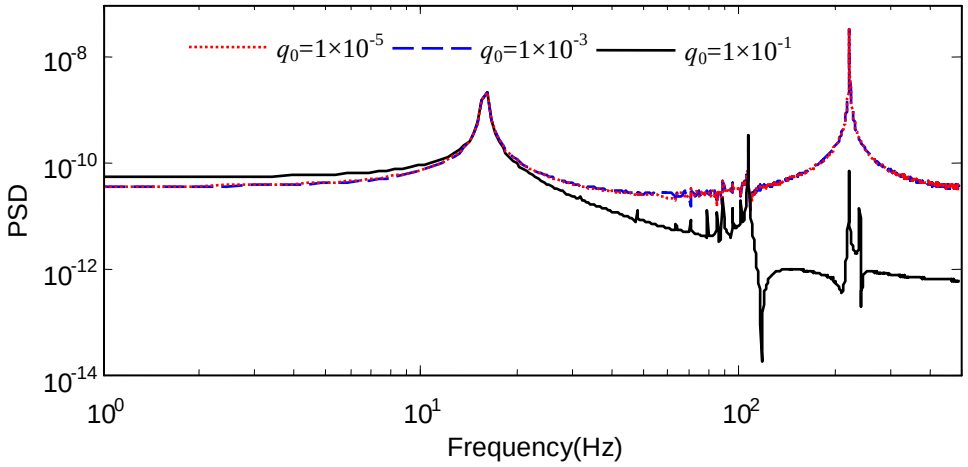

Figure 10. The effects on PSD of the primary structure for different values of q_0.

4. Conclusions

In this study, considering the influences of the gyroscopic and flexible modes of the flywheel and the coupling between the flywheel and the flexible supporting structure on the outputting disturbance, a dynamic coupling model of the flywheel-supporting structure is constructed. And then, a novel NVA, composed of a linear spring in parallel with the Euler buckled beam which function as a negative element, is provided. Based above these models, the fourth-order Runge-Kutta method are used to solve the dynamic equations of the flywheel-NVA-supporting structure. According to the calculating results, the following conclusions can be drawn.

(1) The phenomenon of the non-linear energy pumping is excited when the initial velocity of the supporting structure exceeds a specific threshold, and the responses of the flywheel and the supporting structure are all suppressed evidently. And the non-linear energy sink disappears when the transfer energy to the NVA less than a limited value.

(2) The NVA can absorb vibration energy from the flywheel and the supporting structure when the non-linear energy pumping is not excited due to the initial inputting value less than the threshold value. In addition, the energy sink can be excited by changing the values of the designing parameters of the NVA, for example, the oblique angle, the initial imperfection and the damping coefficient when the other parameter values keeping unchanged.

(3) Compared with the Power Spectral Density of the supporting structure for different values of the damping coefficient, the non-linear energy pumping is excited when the damping coefficient satisfies certain conditions.

(4) The oblique angle of the Euler buckled beam exists an optimal value, and increasing the value of the initial imperfection of the Euler buckled beam improves the suppression effect.

Acknowledgements

This research was supported by the National Natural Science Foundation of China (NSFC) under grant N0. 51405014. In addition, thanks to Professor Michael Brennan and the unknown reviewer who spent valuable time to review our work and made some valuable suggestions.

References

[1] Bialke B, High fidelity mathematical modelling of reaction wheel performance 1998 *Proceedings of the 21st Annual AAS Rocky Mountance Guidance and Control Conference* AAS paper 98-0634 pp 483-496.

[2] Masterson R A, Miller D W, Grogan R L, Development and validation of reaction wheel disturbance models: emprical model 2002 *Journal of Sound and Vibration* 249(3) pp 575-598.

[3] Xu Z D, Wen C H, Zhu J T, Study on the disturbances for the reaction wheel of spacecraft 2013 *Journal of Vibrations, Measurement and Diagnosis* 33(5) pp 881-885. (in Chinese)

[4] Kim D K, Micro-vibration model and parameter estimation method of a reaction wheel assembly 2014 *Journal of Sound and Vibration* 333 pp 4214-4231.

[5] Masterson R A. Development and validation of empirical and analytical reaction wheel disturbance models 1999 *Master dissertation*.

[6] Zhou W Y, Li D X, Luo Q, Liu K, Analysis and testing of microvibrations produced by momentum wheel assemblies 2012 *Chinese Journal of Aeronautics* 25(4) pp 640-649.

[7] Zhou W Y, Research on dynamic modeling and vibration control for the flywheel of spacecraft 2012 *Doctoral dissertation*.

[8] Firth J, Black J, Vibration interaction in a multiple flywheel system 2012 *Journal of Sound and Vibration* 331 pp 1701-1714.

[9] Narayan S S, Nair P S, Ghosal A, Dynamic interaction of rotating momentum wheels with spacecraft elements 2008 *Journal of Sound and Vibration* 315(4-5) pp 970-984.

[10] Zhou W Y, Li D X, Luo Q, Jiang J P, Design and test of a soft suspension system for cantilevered momentum wheel assembly 2012 *Proceedings of the Institution of Mechanical Engineers, Part G: Journal of Aerospace Engineering* DOI: 10.1177/0954410012451415.

[11] Kopidakis G, Aubry S, Tsironis G P, Targeted energy transfer through discrete breathers in nonlinear systems 2001 *Physical Review Letters* 87(16) pp 165501-1-165501-4.

[12] Gendelman O, Manevitch L I, Vakakis A F, M'Closkey R, Energy pumping in coupled mechanical oscillators, Part I: dynamics of the underlying Hamiltonian systems 2001 *Journal of Applied Mechanics* 68 pp 34-41.

[13] Liu H P, Yang J Z, Luo W B, Qian Z Y, Developing the structure and analyzing the effectiveness of a novel Euler buckled beam nonlinear vibration absorber 2015 *Journal of Vibration and Shock*. (Accepted, in Chinese)